Article

Modification of Flux Oxygen Behaviour via Co-Cr-Al Unconstrained Metal Powder Additions in Submerged Arc Welding: Gas Phase Thermodynamics and 3D Slag SEM Evidence

Theresa Coetsee * and **Frederik De Bruin**

Department of Materials Science and Metallurgical Engineering, University of Pretoria, Pretoria 0002, South Africa
* Correspondence: theresa.coetsee@up.ac.za

Abstract: Aluminium metal is avoided as main reactant in submerged arc welding (SAW) because it is easily oxidised in this process. Aluminium is an effective de-oxidiser and can be used to prevent Cr and Co loss to the slag by preventing oxidation of these metals. In our novel application of aluminium metal powder in SAW we demonstrate the modification of flux oxygen behaviour. The Co-Cr-Al-alloyed weld metal total oxygen content is decreased to 180 ppm O, compared to 499 ppm O in the weld metal from the original flux, welded without metal powder additions. The flux oxygen behaviour is modified by the added aluminium powder through the lowering of the original flux-induced partial oxygen pressure in the arc cavity and at the molten flux-weld pool interface. Carbon steel was alloyed to 5.9% Co, 6.3 % Cr and 5.1% Al at 81% Co yield, 87% Cr yield and 70% Al yield. Gas-slag-alloy thermochemical equilibrium calculations confirm the partial oxygen-pressure-lowering effect of aluminium. BSE (backscattered electron) images of the three-dimensional (3D) post-weld slag sample show dome structures which contain features of vapour formation and re-condensation. These features consist of small spheres (sized less than 10 μm) and smaller needle-shaped particles coalescing into a porous sphere. EDX analyses show that the spheres consist of Si-Na-K-Fe-Mn-Co-Cr oxy-fluoride and the needles consist of low oxygen Si-Al-Ca-Mg-Na-K-Fe-Mn-Co-Cr oxy-fluoride. The element distribution and speciation data from the EDX analyses confirm modification of the flux oxygen behaviour via aluminium powder addition in lowering the partial oxygen pressure, which in turn prevents oxidation of Cr and Co and minimise losses to the slag.

Keywords: pyrometallurgy; powder; cobalt; chromium; oxygen control; aluminium; welding

1. Introduction

Submerged arc welding (SAW) is mainly used in heavy engineering industries as a method of joining thick steel plates at high productivity rates [1]. SAW is also used as high productivity method in the application of expensive, specialist cladding materials onto low-cost substrate materials; examples include the application of hard-facing layers onto softer steel substrate and the cladding of reactor vessel interior surfaces with corrosion-resistant materials [2]. SAW process requirements may be different depending on the application. For example, considerable weld metal penetration is required in quality weld joints compared to low weld metal penetration and high surface spread in cladding applications. The SAW process fundamentals remain the same despite these different process requirements in different applications.

The flux applied in SAW serves several functions essential to the pyrometallurgical reactions in the process. One such essential function is the control of total weld metal oxygen (ppm O). It was shown that high impact toughness is maintained in the weld metal if the total oxygen content is within the band of 200 ppm to 500 ppm O [3]. The initial level of total ppm O entering the weld pool via molten weld wire droplets was measured as 2000–3000 ppm O [4,5]. It has been experimentally shown that the dissociation of oxides in

the molten flux (slag) at the high temperatures prevailing in the arc cavity is the only source of this 2000–3000 ppm O [6]. It is reasonable to expect that the oxides' arc plasma stability order must follow the oxides' thermodynamic stability order at the high temperatures prevailing in the arc cavity, 2000 to 2500 °C [7,8]. However, experiments have shown that this is not the case and that there is a unique arc plasma stability order for the oxides typically applied in SAW fluxes. The weld-metal ppm O formed from different oxide–CaF_2 flux mixtures was measured in SAW tests done under argon gas [9]. Higher weld-metal ppm O confirms that the particular metal oxide in the oxide-CaF_2 flux is less stable in the arc because it dissociates in the arc plasma to release oxygen. This work concluded that the oxide arc plasma stability order from the most stable oxide to the least stable oxide is: CaO, K_2O, Na_2O, TiO_2, Al_2O_3, MgO, and SiO_2, and that MnO is the least stable oxide [9]. Consequently, the weld metal total ppm O can be lowered by adding more CaF_2 into the flux to dilute the quantity of low-stability oxides in the molten flux (slag). Empirically determined measurements were used to construct the widely employed trend line of flux composition basicity index, the BI, as expressed in Equation (1), vs. weld metal total ppm O [10]. Based on this trend line, at flux BI values in excess of 1.5 the weld metal total ppm O is constant at 250 ppm O [10]. The weld metal hydrogen content is also minimised at these high flux basicities [7,10].

$$\text{BI} = \frac{\%CaF_2 + \%CaO + \%MgO + \%BaO + \%SrO + \%Na_2O + \%K_2O + \%Li_2O + 0.5(\%MnO + \%FeO)}{\%SiO_2 + 0.5(\%Al_2O_3 + \%TiO_2 + \%ZrO_2)} \tag{1}$$

In addition to the formulation of fluxes for oxygen and hydrogen control, flux chemistry is formulated to achieve targeted element transfer levels from the slag to the weld metal [11–14]. Therefore, any changes to the formulation and application of SAW consumables will influence the SAW chemical reactions and should be tested to quantify the effects on process chemistry.

Chromium has a high affinity for oxygen and is therefore not easily transferred across the arc [15]. Instead, chromium is typically alloyed into the weld pool via weld wire, often with nickel as stainless steel wire. A few studies have reported on chromium loss to the slag for different flux formulations applied in SAW [16,17]. In both studies, the effect of flux basicity was found to be the main factor in chromium transfer to the weld metal. Chromium loss was observed from the Cr_2O_3-containing flux and ascribed to Cr_2O_3 volatilisation at the high temperatures in the welding process [16]. The weld metal total ppm O values attained were relatively high at 470 ppm O to 1450 ppm O, indicating a high level of dissociation of flux Cr_2O_3 in the arc plasma. In agreement with the results, the flux Cr_2O_3 was included in Equation (1) as an acidic oxide, similar to TiO_2. Another study investigated the effect of flux chemistry on chromium loss from low alloy carbon steel weld metal [17]. The raw flux contained zero chromium oxides. Chromium loss was negligible when reducing flux (CaF_2 containing flux) was used, compared to increased chromium loss seen with the application of more oxidising flux (FeO or MnO containing flux with no CaF_2 added). The weld metal ppm O changed in tandem with the chromium loss trends at 230–300 ppm O from the reducing flux (40% SiO_2-MnO-CaF_2) vs. 553–700 ppm O from the oxidising flux (40% SiO_2-MnO-FeO) [17]. The results indicate that oxygen released from the flux in the arc cavity plays an important role in chromium loss from the weld metal and/or slag.

Cobalt has a low affinity for oxygen and is therefore typically added into the SAW weld pool from alloyed weld wire. Cobalt is used in combination with chromium in hardfacing applications of the well-known cobalt–chromium based alloy, Stellite [2]. It has been reported that cobalt and nickel vaporisation levels are higher in laser cladding applications than in arc welding methods. The initial metal vapours are quickly oxidised to nickel oxide and cobalt oxide in the atmosphere [18]. Cobalt is not only used in cladding/hardfacing applications. For example, cobalt (3% Co) is added to high temperature steel with 9% Cr to improve creep resistance in newly developed steel grades for ultra-supercritical (USC) power generation plant construction applications [19,20]. Hardfacing alloys may be

applied in SAW as pre-alloyed metal powders [21]. Similar to nickel-containing pre-alloyed powders, the SAW application of iron-based cobalt-containing pre-alloyed powders at up to 40% Co was demonstrated. No cobalt yield data was presented. In the same work, in the cladding application of Fe-Ni-Cr-Mo pre-alloyed powder, the yield values from the powder to the weld metal were 57–78% Ni and 56–76% Cr [21]. Because Ni and Co have similar oxygen affinity, melting and boiling points, and vapor pressures vs. temperature, it may be expected that cobalt's yield to the weld metal is similar to that of nickel. Since cobalt is expensive, currently at $US 27/lb, and price increases are expected due to cobalt demand associated with Li-ion battery manufacture for electric cars, it is important to maximise Co yield to the weld metal [22,23]. Therefore, investigation of cobalt's chemical behaviour in SAW is of importance, irrespective of its application in cladding or joining operations.

Aluminium is not typically added in large quantities to steel but recent developments of low density/high-entropy steels and low-density stainless steels require high quantities of aluminium in their formulations [24,25]. Therefore, it is expected that combinations of alloying elements with aluminium will become increasingly important in expanding the application of SAW to these newer steel grades. Manufacturing of weld wires of specific compositions is expensive and time consuming. Furthermore, available weld-wire compositions are limited and cannot match all desired alloy compositions. A closer-matched alloying of the weld metal may be accomplished if metal powder is applied to the welding process to achieve the desired weld metal composition [21]. Pre-alloyed powder manufacturing is also time consuming and suffers from limits in matching capabilities. A better cost alternative is the application of unconstrained metal powders in SAW. Unconstrained metal powders refer to non-alloyed metal powders which are not constrained in tubular wire, such as flux cored and metal cored wire.

Aluminium metal is avoided as a main reactant in SAW because it is easily oxidised in this process. In our novel application of aluminium metal powder in SAW we demonstrate the modification of flux oxygen behaviour to control the weld metal total ppm O, as in our previous works [26–33]. Because alloying element yield is dependent on the flux-induced partial oxygen pressure, the element yield can be improved by de-oxidiser application. Here we apply aluminium to prevent Cr and Co loss to the slag by preventing oxidation of these metals.

In this research, we apply a combination of Co, Cr and Al powders to measure the alloying element yield numbers and weld metal total ppm O. These numbers are compared to those from our previous study on Co and Al metal powders applied under the same SAW conditions [32]. The main objective of the current study is the demonstration of the application of unconstrained Co, Cr and Al powders in SAW, to alloy the weld metal and control the weld metal oxygen content. The secondary objective is to explain how the Co-Cr-Al metal powders modify the flux oxygen behaviour.

2. Materials and Methods

2.1. Welding Tests

Welding tests were made as bead-on-plate weld runs of typically 260 mm length onto 350 mm length steel plate. The plate thickness was 12 mm, and the plate width was 300 mm. Welding parameters were 500 A and 28 V at 42 cm/min travel speed to provide a heat input value of 2.0 kJ/mm. Welding was done DCEP (direct current electrode positive) with weld wire of 3.2 mm diameter.

One SAW test run was made without the addition of metal powders in order to generate a base case (BC) weld for comparison to welds made with metal powder additions. The welds made with metal powder additions are named with MP labels. The welding parameters stated above were applied in all welding tests. The metal powders consisted of chemically pure powders sourced from commercial metal powder suppliers. Powder additions per weld test consisted of aluminium, chromium, and cobalt powders of 7 g each. The weld metal cross-sections are shown in the Figure 1 photograph. The MP7 weld metal was made with Al and Co metal powders as described in our previous study [32]. The

MP9 weld metal was made with Al, Co and Cr metal powders and is analysed in detail in this work.
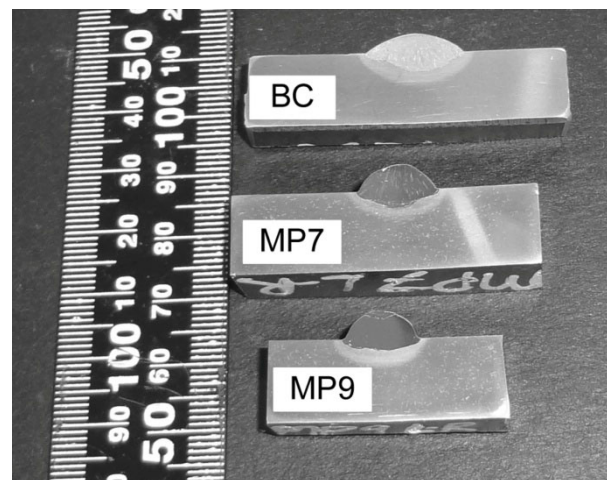

Figure 1. Photograph of BC, MP7 and MP9 weld metal cross-sections.

2.2. Materials and Analyses

Structural steel of grade (S355J2 + N) was used as base plate material, since this is a widely available steel formulation in South Africa. The chemical analyses of the base plate steel and weld wire are displayed in Table 1. Analysis method details were previously described in our prior publication [34].

Table 1. Carbon steel base plate and weld wire compositions (mass%) [27].

	%C	%Si	%Mn	%O	%Al	%P	%S	%Ti	%Cu	%Cr	Balance
Plate	0.120	0.155	1.340	0.0007	0.067	0.019	0.007	0.005	0.030	0.160	Fe
Wire	0.110	0.137	0.990	0.0003	0.000	0.009	0.023	0.000	0.140	0.000	Fe

One commercial flux formulation was used in all the welding tests. The flux is an aluminate basic flux with a flux basicity of 1.4, as expressed as in Equation (1). The agglomerate particle size fraction is 0.2 to 1.6 mm. The flux bulk chemical composition is shown in Table 2 as reported in a previous detailed chemistry and mineralogy investigation [34]. An important consideration in the selection of a flux for this work is the thermodynamic stability of the flux in the presence of aluminium metal. Therefore, the aluminate basic flux was selected following initial testing of different fluxes [34]. Metal powders of pure Al (99.7% Al) supplied by Sigma-Aldrich, pure Co (99.9% Co) supplied by GoodFellow and pure Cr (99.0% Cr) supplied by Alfa Aesar were used.

Table 2. Flux bulk chemical composition (mass%) [27].

MnO	CaO	SiO_2	Al_2O_3	CaF_2	MgO	FeO	TiO_2	Na_2O	K_2O
6.8	0.1	19.6	24.9	17.9	22.2	2.4	1.0	1.6	0.2

2.3. Thermochemical Calculations for Gas Phase Reactions

The Equilib module in FactSage 7.3 thermochemical software was applied to calculate the equilibrium of gas, slag, and metal powder inputs as equilibrium phases of gas, molten flux (slag) and molten alloy. This gas-slag-metal equilibrium model is similar to the simulation model previously successfully applied to calculate the carbon steel weld metal total ppm O in SAW for different flux formulations [35]. The proportion of the feed aluminium quantity that possibly participated in the gas reactions was varied to gauge

the role of aluminium in the gas phase reactions. The thermodynamically predicted gas phase species from these calculations were used to interpret the likely gas phase reaction changes due to chromium, cobalt and aluminium added to the SAW process. The FToxid, FSstel and FactPS databases were selected, and the selection made for inclusion of plasma species [36]. The calculation results are discussed in Section 4.1.

3. Results

3.1. Weld Metal Analyses

Table 3 displays three bulk weld metal compositions. All weld runs were made by using the same welding parameters, as noted in Section 2.1. The only differences are the absence of metal powders in the base case weld run (BC), the test run with Al and Co metal powder addition (MP7) and the test run with Al, Co, and Cr metal powder addition (MP9). The MP7 weld run was previously discussed in detail and is shown here for comparison to the MP9 weld test results [32]. Methods of weld metal sample cutting were previously described in detail [32]. Figure 2 displays the SEM micrograph in the geometric centre of the MP9 weld metal cross section. The marked areas were selected for EDS analyses as displayed in Table 4. The EDS analyses in Table 4 confirm alloying of the weld metal with the added metal powders of cobalt, chromium, and aluminium. Details of the SEM equipment used in the EDS analyses were described previously [32].

Table 3. Bulk chemical composition of weld metals (mass%).

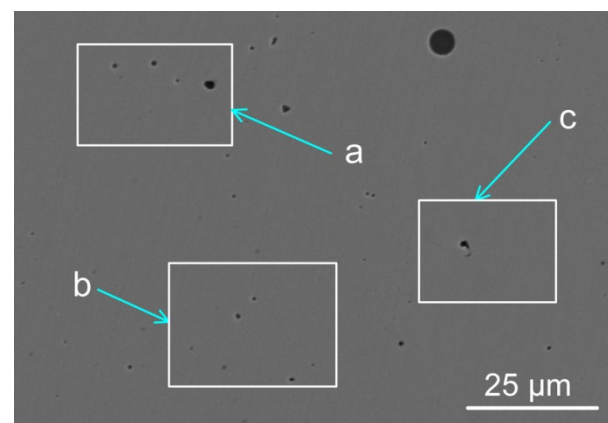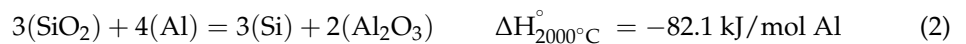|	%C	%Si	%Mn	%O	%Al	%P	%S	%Co	%Cr	%Fe
Base Case	0.110	0.260	1.300	0.0499	0.032	0.022	0.011	0.006	0.110	98.03
MP7	0.105	0.410	1.723	0.0230	4.200	0.023	0.011	5.340	0.163	87.71
MP9	0.097	0.910	1.567	0.0180	5.057	0.023	0.008	5.873	6.300	79.93

Figure 2. Scanning electron microscope micrograph of weld metal areas as marked a, b and c. (See Table 4 below, indicating the analyses per marked phase areas: a, b, and c) ($\times 2460$).

Table 4. SEM-EDS analyses of marked areas in the MP9 weld metal as indicated in Figure 2 (mass%).

	%Si	%Mn	%Al	%Co	%Cr	%Fe
a	0.80	1.60	6.21	7.11	7.01	77.3
b	0.92	1.53	6.00	7.12	7.22	77.2
c	0.93	1.66	5.90	7.25	7.45	76.8

The weld metal analyses data in Table 3 confirm increased silicon and manganese content in MP7 and MP9 weld metal, as compared to the BC weld metal. This is due to aluminothermic reduction of MnO and SiO_2 from the slag, as identified in our previously reported work on aluminium-assisted alloying of different metal powders in

SAW [26–33]. Therefore, the aluminothermic reduction reactions in Equations (2) and (3) also occurred in the MP9 weld run. In addition, the aluminothermic reduction reactions in Equations (4) and (5) are also considered possible, although the extent of these reactions is less clear than that of the reactions in Equations (2) and (3). It was confirmed from our previous similar works on different metal powder combinations with aluminium, that FeO is formed from oxidation of iron by the excess oxygen transferred from the arc cavity [37,38]. This FeO may also be reduced by aluminium powder via reaction (4) to control the oxygen potential at the weld pool-slag interface [26–33]. In the same way, chromium oxide can be reduced by aluminium via Equation (5) [28].

$$3(SiO_2) + 4(Al) = 3(Si) + 2(Al_2O_3) \qquad \Delta H^{\circ}_{2000°C} = -82.1 \text{ kJ/mol Al} \qquad (2)$$

$$3(MnO) + 2(Al) = 3(Mn) + (Al_2O_3) \qquad \Delta H^{\circ}_{2000°C} = -248.4 \text{ kJ/mol Al} \qquad (3)$$

$$3(FeO) + 2(Al) = 3(Fe) + (Al_2O_3) \qquad \Delta H^{\circ}_{2000°C} = -416.5 \text{ kJ/mol Al} \qquad (4)$$

$$3(CrO) + 2(Al) = 3(Cr) + (Al_2O_3) \qquad \Delta H^{\circ}_{2000°C} = -326.6 \text{ kJ/mol Al} \qquad (5)$$

( ): liquid.

The effect of added metal powders, specifically the de-oxidising effect of aluminium, is seen from the differences in weld metal total ppm O as reported in Table 3. Weld metal total ppm O is significantly lowered from the BC test run value of 499 ppm O to 230 ppm O in the MP7 weld metal, and to 180 ppm O in the MP9 weld metal.

3.2. Mass Balance

A mass balance was done to quantify the yield of cobalt, chromium, and aluminium from the metal powders added to the weld metal. The mass balance measurements and calculations procedure were described in detail in our previous works [26,29–33]. The %yield of Co, Cr and Al from metal powder to weld metal can be calculated once the gram mass of Co, Cr and Al added to the weld metal have been calculated from the mass balance. The latter values are displayed in Table 5. The %yield is calculated as a percentage of the 7 g of Co or Cr or Al added to the weld run. Table 5 shows that the MP9 yield values were calculated as 70% Al yield, 81% Co yield and 87% Cr yield. The yield value of Co is higher in the MP9 weld run, compared to the MP7 weld run made in the absence of chromium metal powder. The same trend holds for the %Al yield. From these results two clear observations are highlighted. Firstly, the %yield values of Co and Cr are not close to 100% as is typically implied in literature. Secondly, when chromium is added to the weld run, the Co yield is improved. The likely reasons for these observations are presented in the discussion section below.

Table 5. Mass balance numbers and percentage yield calculation results for Al, Co and Cr.

	Al (g)	Co (g)	Cr (g)	Powder (g)	Wire (g)	Base Plate (g)	Weld Metal (g)	%DR$_{(wire + MP)}$	%Al Yield	%Co Yield	%Cr Yield
MP7	3.9	5.0	0	8.9	51.1	33.5	93.5	64	55	70	0
MP9	4.9	5.7	6.1	16.8	53.2	27.4	97.4	72	70	81	87

3.3. Quantification of the Exothermic Reactions with Aluminium

Alumina formed as product in the reactions displayed as Equations (2) and (3) was easily absorbed into the molten flux because these reactions occurred at the molten flux-weld pool interface [26–33,37]. Calculation of the exothermic reaction heat contributions from Equations (2) and (3) is possible once the mass Mn and mass Si contributed from these reactions to the weld metal are quantified, using Equation (6). This calculation procedure has been reported previously [26,29–33]. Equation (6) shows calculation of the mass of Mn added from aluminothermic reduction, (M_{Mn}). The inputs to Equation (6) are the weld metal mass, (M_{wm}), the %Mn in the weld metal from Table 3, and the dilution ratio value, (%DR$_{(wire + MP)}$) at 50% for the base case as stated previously [26,29–33]. The

square bracketed terms in Equation (6) represent the calculation of the BC weld metal nominal composition.

$$M_{Mn} = (M_{WM}) \left(\frac{\%Mn_{WM}}{100} - \left[\frac{\%DR_{wire}}{100} \times \frac{\%Mn_{wire}}{100} \right] - \left[\left(1 - \frac{\%DR_{wire}}{100} \right) \times \frac{\%Mn_{BP}}{100} \right] \right) \qquad (6)$$

M = mass (gram); M_{WM} = mass Mn (gram); $\%Mn_{WM}$ = %Mn in weld metal; $\%DR_{wire}$ = % of weld metal contributed by weld wire in the Base Case (BC); $\%Mn_{wire}$ = %Mn in weld wire; $\%Mn_{BP}$ = %Mn in Base Plate (BP); WM = weld metal; BP = base plate; Wire = weld wire.

The exothermic heat from the reactions in Equations (2) and (3) were calculated from the reaction enthalpy values as displayed next to Equations (2) and (3). A simplified translation of the kJ values is made by using the heat capacity of steel (0.460 kJ/kg K) to calculate the expected increase in weld metal temperature due to these reactions. From the numbers shown in Table 6, it is seen that small gram quantities of SiO_2 and MnO were reduced into the weld metal via the reactions in Equations (2) and (3). However, the exothermic heat released from these reactions is sufficiently large to significantly increase the weld metal temperature by 91 °C as displayed in the last column of Table 6. This value may be compared to a 58 °C temperature increase calculated previously for the MP7 weld metal [32]. Because this heating effect is instantaneous, the heating effect is significant in the welding process. The exothermic heat may contribute to the melting of metal powders to facilitate its incorporation into the weld pool, and so increase overall process productivity.

Table 6. Exothermic heat added to the weld pool from reactions (2) and (3).

	SiO_2 (g)	MnO (g)	Al (g)	Reaction (2) (kJ)	Reaction (3) (kJ)	Reactions (2) & (3) (kJ)	Weld Metal ΔT (°C)
MP7	0.53	0.67	0.49	−0.96	−1.57	−2.53	58
MP9	1.59	0.50	1.08	−2.90	−1.18	−4.08	91

The weld pool solidification time plays an important role in SAW because it sets the time available for oxide inclusions to float from the weld pool to the molten slag-weld pool interface, eventually being absorbed into the molten slag [39]. Therefore, these physical phenomena play a role in setting the weld metal total ppm O. The weld pool cooling time, set by the difference between the weld pool liquidus and solidus temperature, may be different for differing weld pool chemistries. Figure 3 shows the cooling curves for the BC, MP7 and MP9 weld metal compositions. The cooling curves were calculated in FactSage 7.3 thermochemical software, using the Equilib module with FToxid and FSstel databases selected [36]. From Figure 3 it is seen that the solidus temperatures of MP7 and MP9 weld metals are within 50 °C of each other. In comparison to the BC weld metal cooling curve, it is expected that the MP7 and MP9 weld pool cooling time will be longer. This difference will at least in part contribute to a lower ppm O in the MP7 and MP9 weld metal as compared to the BC weld metal.
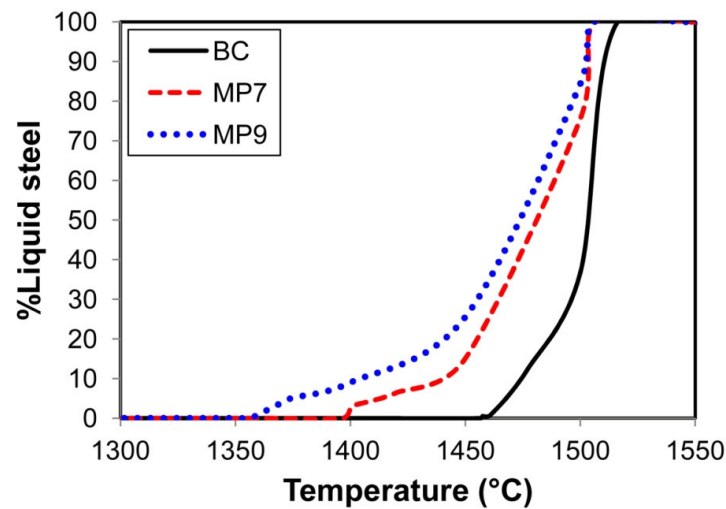
Figure 3. Solidification curves for MP9, MP7 and BC weld metal compositions from Table 3.

3.4. Chromium and Cobalt Speciation and Distribution in the Slag

The post-weld slag ribbon is displayed in the photographs in Figure 4. Cross-sections samples of the slag ribbon were studied by SEM as 2D (two-dimensional) polished section and as 3D (three-dimensional) fractured cross-section surface.
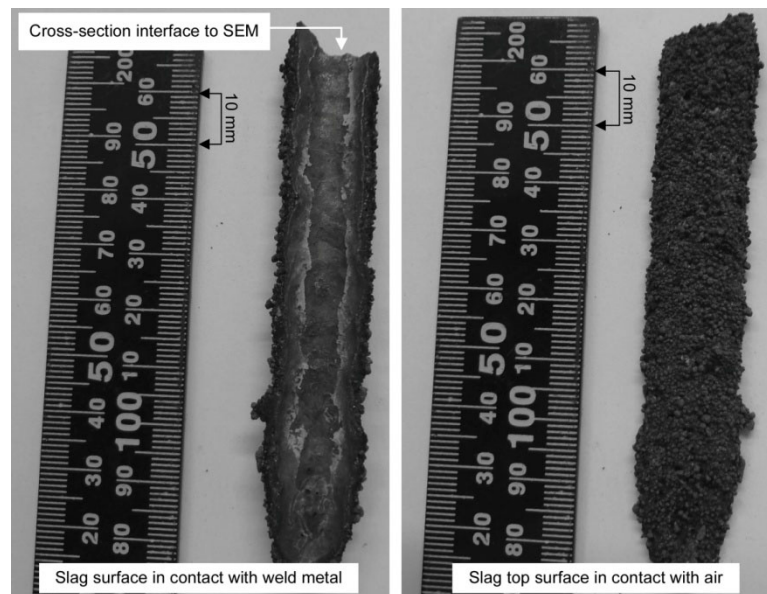

Figure 4. Photographs of post-weld slag ribbon from MP9 weld.

Speciation and distribution of the elements in the MP9 post-weld slag were investigated. EDX (energy dispersive X-ray) analyses were used to map the elements in the area at the weld metal-slag interface. The major phases in the post-weld slags that formed from aluminium assisted welding with the aluminate basic flux were identified previously as spinel crystals ($MgAl_2O_4$) embedded in an oxy-fluoride glass matrix phase [34,37,38]. The slag area displayed in the BSE (backscattered electron) image in Figure 5a was analysed by EDX as displayed in Figure 5b. From the data in Figure 5b it is clear that only small quantities of chromium are present in the oxy-fluoride matrix glass phase and the solid spinel phase. In comparison, Co is present in the oval-shaped speck which contains no oxygen and some fluoride. This oval-shaped speck contains a mixture of Co, Fe and Cr. Manganese specks appear to be independent of the alloy speck. Therefore, the application of aluminium powder as a de-oxidising element ensures sufficiently reducing conditions at

the weld pool-slag interface to limit the oxidation of chromium and cobalt to their oxides. The result is that any significant loss of these elements as oxides into the slag is prevented by aluminium de-oxidiser additions. The implication is that the loss of chromium and cobalt from the metal powders is expected to be via metallic chromium and cobalt. Table 7 shows the average analysis of the area displayed in Figure 5. It is seen that the concentrations of chromium and cobalt are low to negligible.
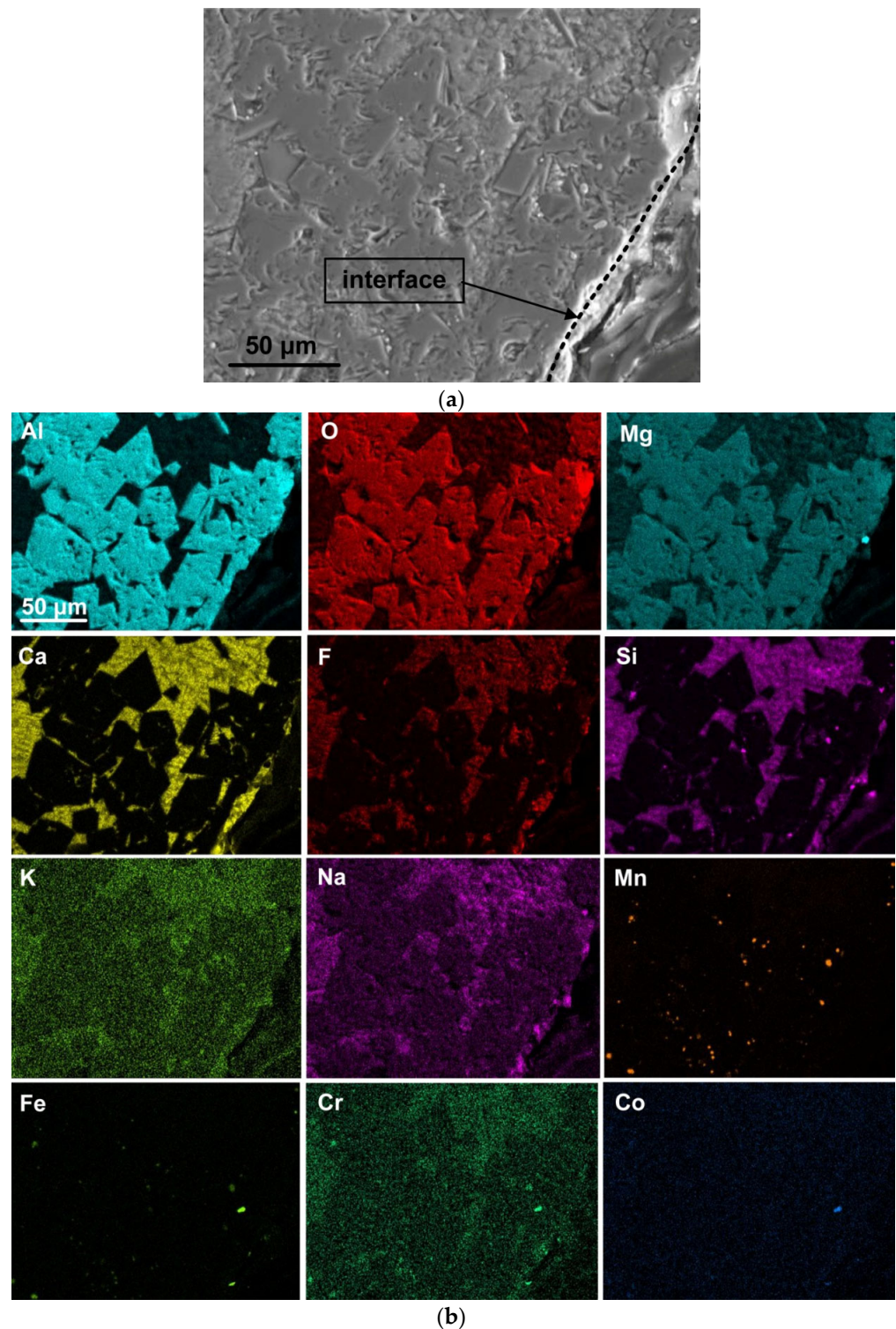

(a)

(b)

Figure 5. (**a**) BSE image of slag area at the weld metal-slag interface in MP9 post-weld slag, and (**b**) EDX maps of slag area in (**a**) at the weld metal-slag interface in MP9 post-weld slag.

Table 7. Average EDS analyses of post-weld slag area in Figure 5 (mass%).

	%F	%O	%Al	%Si	%Mg	%Ca	%Mn	%Fe	%Ti	%Na	%K	%Cr	%Co
Slag	8.0	47.2	20.6	2.8	12.6	6.6	0.8	0.3	0.3	0.6	0.1	0.1	0.0

A SEM study of three-dimensional (3D) slag samples shows up more details, in particular evidence of vapour formation in dome structures as displayed in Figure 6a. The details shown in the larger magnification BSE image in Figure 6b confirm small sized porous structures which likely formed due to vaporisation and re-condensation of the particular elements. The EDX analysis maps of the area in Figure 6b are shown in Figure 6c. The 3D needle structure consists of Si-Al-Ca-Mg-Na-K-Fe-Mn-Co-Cr oxy-fluoride, whilst the smaller spheres at the base of the 3D needle structure consist of Si-Na-K-Fe-Mn-Co-Cr oxy-fluoride. The background matrix phase surrounding the smaller spheres is also oxy-fluoride of Si-Al-Ca-Mg-Na-K-Cr without Co, Fe and Mn. Although in low concentration, both Co and Cr are present in these structures and these elements in the slag structures could only be sourced from the added metal powders. Comparison of the average analysis in Table 8 to that of the two-dimensional (2D) slag area in Table 7 confirms that the 3D structures are dominated by low oxygen content oxy-fluorides with Si- Fe-Mn as the main constituents.
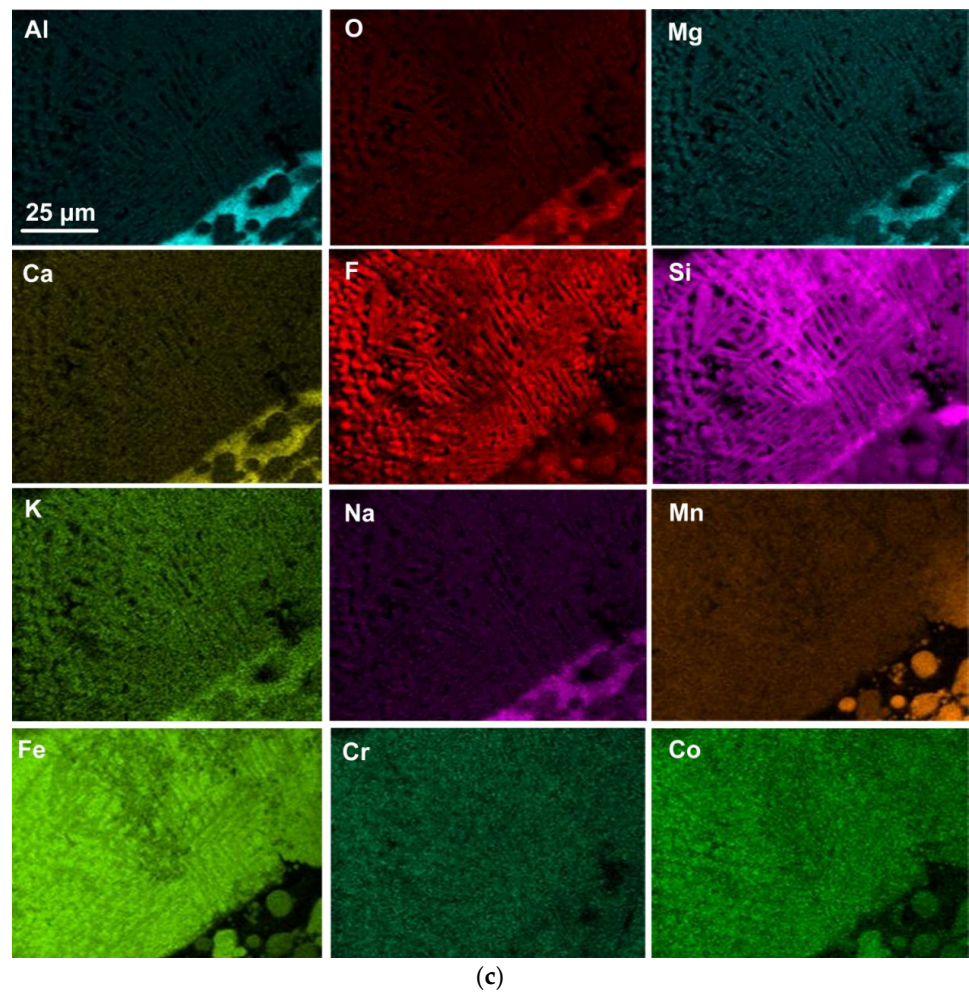

(**a**)

(**b**)

Figure 6. *Cont.*

(c)
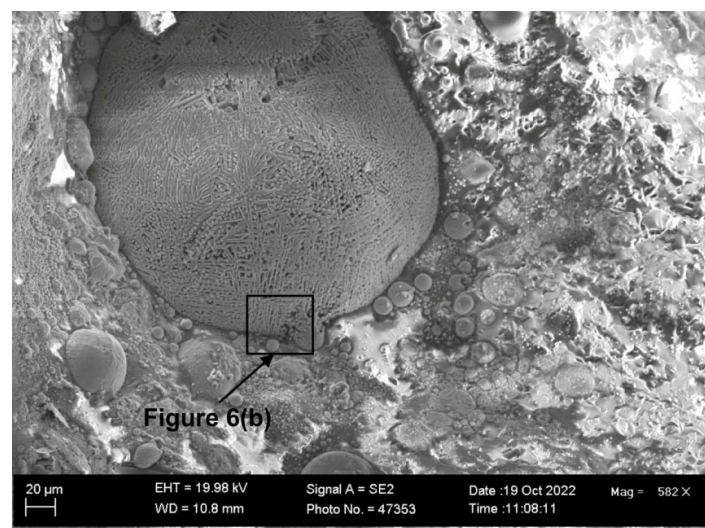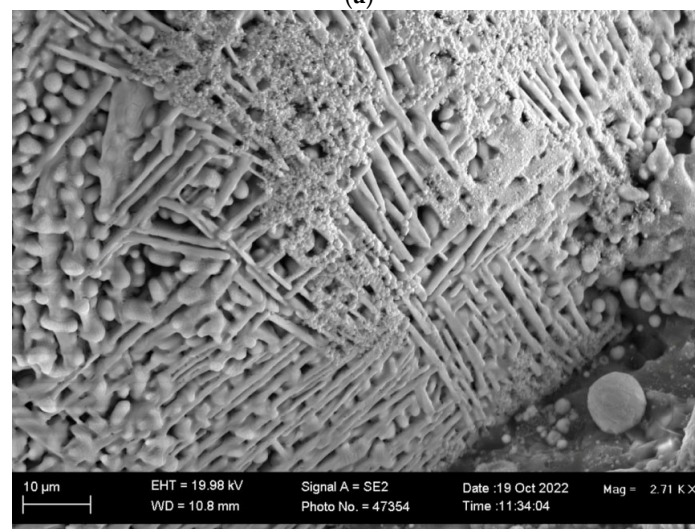
Figure 6. (**a**) BSE image at 582× magnification showing a 3D needle structure within the slag dome in the MP9 post-weld slag; (**b**) BSE image at 2710× magnification of the 3D structure marked in Figure 6a; and (**c**) EDX maps of 3D slag structures in (**b**).

Table 8. Average EDS analyses of 3D slag structures in Figure 6b.

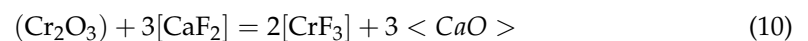|	%F	%O	%Al	%Si	%Mg	%Ca	%Mn	%Fe	%Ti	%Na	%K	%Cr	%Co
Slag	9.0	5.2	1.8	31.7	0.9	0.1	10.6	36.9	1.0	1.6	0.0	0.5	0.5

4. Discussion

Weld metal total ppm O is sourced from the oxides contained within the flux, and this oxygen is transferred from the molten flux to the weld metal via gas phase reactions in the arc cavity [4–6]. Gas-slag-metal equilibrium calculations were demonstrated to be an accurate simulation model for total weld metal ppm O for different flux chemistries in carbon steel SAW tests [35]. In comparison, slag-metal equilibrium calculations for the same inputs provided poor results [35]. Therefore, gas phase reactions are important in the interpretation of any modifications of the SAW process. In this work and our previous studies, aluminium powder is applied in SAW to control the weld metal total ppm O [26–33]. Aluminium as de-oxidiser lowers the partial oxygen pressure at the molten flux-weld pool interface [26–33]. In addition, aluminium is also present in the arc cavity, and can therefore also lower the oxygen partial pressure in the arc cavity [32,33,40]. It has been conclusively shown that Al transfers from the flux via the gas phase in the arc cavity [40]. In the following section, thermochemical calculations of the gas-slag-metal

powder equilibrium are used to investigate the likely gas phase reaction changes due to chromium, cobalt and aluminium powders added to the SAW process.

4.1. Thermochemical Equilibrium Calculations

Consideration of combinations of likely simplified fluoride-based chemical reactions as displayed in Equations (7)–(12) below has been reported previously by considering the Gibbs free energy for each reaction at 1600 to 2500 °C [26,32,33]. The conclusions were that for all the metals typically applied in SAW, the metal vapour will most probably react with fluorine gas as displayed in Equations (7) and (8), and that reactions of metal oxides with CaF_2 vapour as in Equations (9) and (10) are less probable. The high stability of Al-fluorides ensures that reactions similar to Equations (11) and (12) are highly probable, namely the reaction of Al vapour with the less thermodynamically stable metal fluorides to form $AlF_3(g)$ and metal vapour. The Gibbs free energy calculations showed that formation of $CrF_3(g)$ as displayed in Equation (8) is more probable than formation of $CrF_2(g)$ in the same type of reaction. This is the reason for using $CrF_3(g)$ in Equations (8), (10) and (12).

$$[Co] + [F_2] = [CoF_2] \tag{7}$$

$$2[Cr] + 3[F_2] = 2[CrF_3] \tag{8}$$

$$(CoO) + [CaF_2] = [CoF_2] + <CaO> \tag{9}$$

$$(Cr_2O_3) + 3[CaF_2] = 2[CrF_3] + 3 <CaO> \tag{10}$$

$$2[Al] + 3[CoF_2] = 2[AlF_3] + 3[Co] \tag{11}$$

$$[Al] + [CrF_3] = [AlF_3] + [Cr] \tag{12}$$

( ): liquid; [ ]: gas; < >: solid.

In addition, considering the vaporisation curves of the metallic elements present in the welding process as displayed in Figure 7, shows that the order of ease of vaporisation is from highest to lowest: Mn, Al, Cr, Fe, Co and lastly Si. The vapour pressure curves in Figure 7 were calculated in FactSage 7.3 thermochemical software using the ELEM data base in the Reaction module [36]. Figure 7 confirms that aluminium is easily vaporised at the high temperatures prevailing in the arc cavity, 2000 to 2500 °C [7,8]. The data in Figure 7 indicates that direct metal vaporisation is possible at the high temperatures in the arc cavity, especially from Al metal.
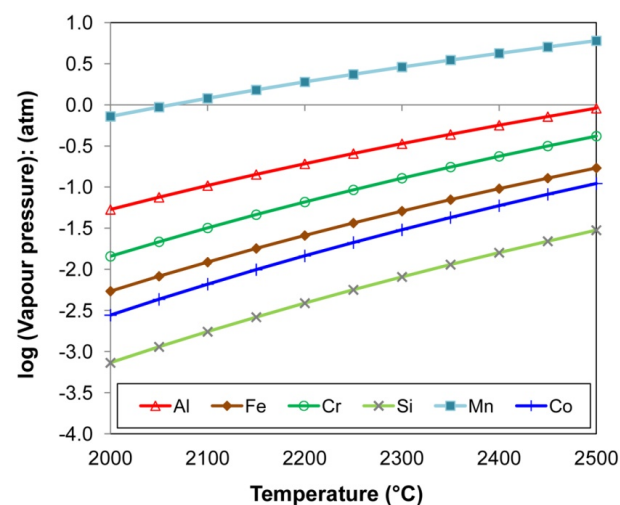

Figure 7. Vapour pressure of pure metals Mn, Al, Cr, Fe, Co, Si vs. Temperature.

Because the above reaction and vaporisation possibilities were investigated for pure substances, more realistic thermochemical calculations were made to investigate the prob-

ability of species formation, especially in the gas phase. The Equilib module in FactSage 7.3 thermochemical software was used to calculate the gas-slag-metal powder equilibrium between the molten flux (slag) and the alloy powders. Calculation details are summarised in Section 2.3.

The flux input composition is that shown in Table 2 and the flux mass input is equal to the slag mass measured for the post-weld slag. The cobalt and chromium weld input masses of 7 g each were specified as inputs to the calculation. The aluminium input mass in the calculation was varied between zero, 50% and 100% of the maximum of 5.9 g aluminium. Since the mass balance calculations showed that 1.08 g of the input 7 g of aluminium was consumed in the reactions in Equations (2) and (3), the maximum mass of added aluminium powder remaining for gas phase reactions is 5.9 g Al. The calculated gas compositions and quantities are summarised in Table 9. The calculated loss percentages of Al, Co and Cr to the gas phase and the gas phase partial oxygen pressure (P_{O2}) values are summarised in Table 10. The similar calculation results for MP7 inputs as presented previously are used in comparison to the MP9 results in the following discussion [32].

Table 9. MP9 gas composition (volume %) output from gas-slag-metal powder equilibrium at 2500 °C calculated in FactSage 7.3 thermochemical software (Equilib module) [36].

Gram Al	%MgF$_2$	%MgF	%Mg	%AlF$_3$	%AlF$_2$	%AlF	%CaF$_2$	%NaF	%Na	%Mn	%MnF$_2$	%Co	%SiO	%Cr	%CrF$_3$
zero	13	9	10	2	4	6	12	5	5	7	<1	6	8	7	1
2.96	4	7	19	<1	4	15	5	2	4	7	<0.5	5	12	10	<0.5
5.92	1	4	24	<0.5	2	22	2	1	4	7	<0.1	4	15	11	<0.1

Table 10. MP9 expected metals loss to gas according to gas-slag-metal powder equilibrium at 2500 °C calculated in FactSage 7.3 thermochemical software (Equilib module) [36].

Gram Al	mass %Co to gas	mass% Cr to gas	mass% Al to gas	P_{O_2} (atm)
zero	10	12	0	1.3×10^{-6}
2.96	13	24	57	2.5×10^{-7}
5.92	16	37	51	7.7×10^{-8}

Comparison of the gas-slag-metal equilibrium calculation outputs for the MP7 and MP9 weld test runs are shown in Figures 8–10. The only difference in inputs between the MP7 and MP9 welding tests is the alloying powders added: Al and Co in MP7 vs. Al, Cr and Co in MP9. In Figure 8 it is seen that the calculated proportion aluminium in the gas phase is similar for both the MP7 and MP9 test inputs. In contrast, the calculated cobalt loss to the gas phase is less for MP9 than for MP7 test inputs, see Figure 9. This indicates that the addition of chromium plays a role in the cobalt loss reactions. Figure 10 summarises the calculated gas phase partial oxygen pressures and highlights that chromium metal powder also performs as a de-oxidiser element. This is seen at zero percent aluminium-reacted, indicating a lower partial oxygen pressure for MP9 than for MP7 input conditions at partial oxygen pressure (P_{O2}) at 1.3×10^{-6} atm vs. 6.3×10^{-5} atm. The partial oxygen pressure values are of the same order of magnitude when 50% and 100% aluminium were included in the equilibrium calculations. The increased quantity of calculated chromium in the gas phase is associated with a small decrease in quantity of aluminium loss to the gas phase from 57 mass% to 51 mass%, see Table 10. It appears that some aluminium metal vaporisation may be substituted by chromium metal vaporisation.
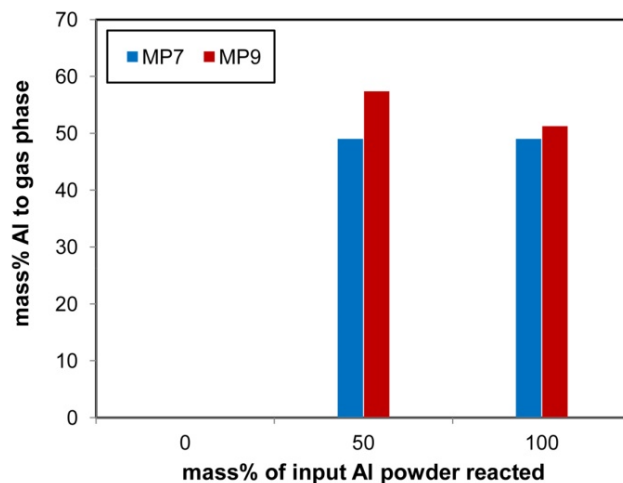
Figure 8. Expected aluminium loss to gas according to gas-slag-metal powder equilibrium at 2500 °C: MP7 to MP9 comparison.
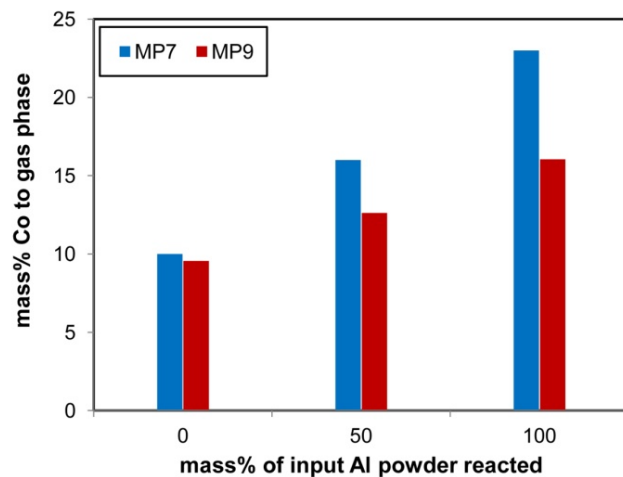

Figure 9. Expected cobalt loss to gas according to gas-slag-metal powder equilibrium at 2500 °C: MP7 to MP9 comparison.
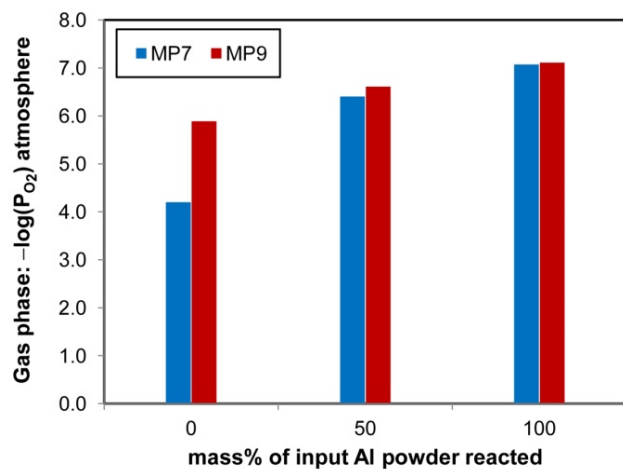

Figure 10. Calculated gas phase partial oxygen pressure according to gas-slag-metal powder equilibrium at 2500 °C: MP7 to MP9 comparison.

It is noted that these are thermochemical equilibrium calculation results for the maximum temperature reported in the arc cavity (2500 °C) and are only an indication of probable reaction trends. The values are not presented here as absolute values, but as an aid in the interpretation of the flux oxygen behaviour changes due to the different metal powder additions made in the welding tests. Based on the insights from the discussion above, our SAW reaction flow diagram is updated for Al, Co and Cr metal powder additions as shown in Figure 11.
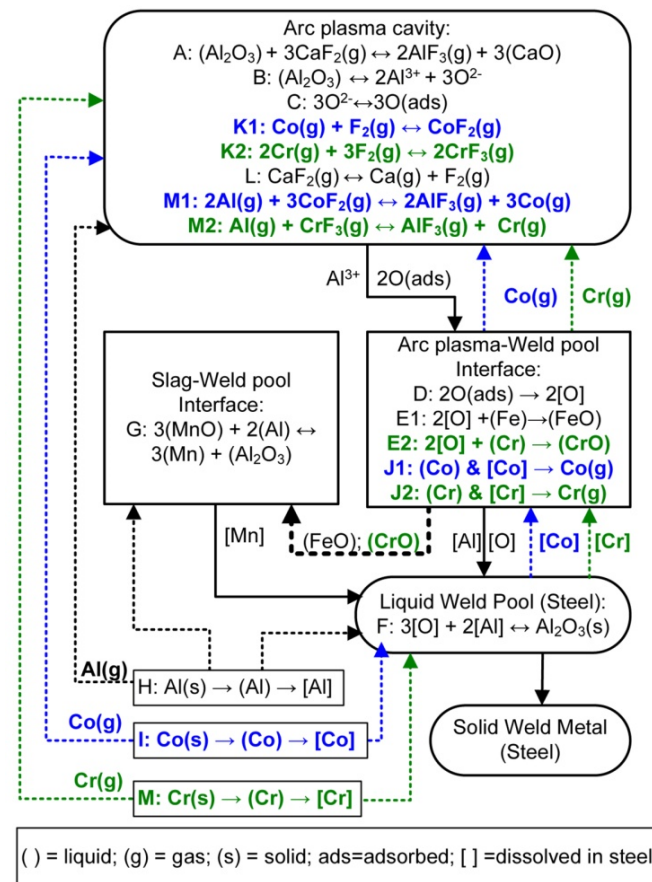
Figure 11. SAW reaction flow diagram with Al, Co and Cr powder additions.

4.2. SAW Reaction Flow Diagram with Al, Co, Cr Metal Powder Additions

The following discussion incorporates the findings from the above results and discussion on gas-based reactions into our SAW reaction flow diagram (Figure 11). Reaction steps A to E are as presented from previous works and represent the transfer of oxygen from the molten flux (slag) to the weld pool [4–6,16,35,41]. Reaction A corresponds to the same type of reaction as in Equations (9) and (10), the reaction of Al_2O_3 with $CaF_2(g)$ to form $AlF_3(g)$ and CaO. This type of reaction is often written in texts on fluoride-based welding fluxes, although the lowest Gibbs free energy values for Al-fluoride formation is via the reaction $Al(g)$ with $F_2(g)$, similar to Equations (7) and (8), [26,32,33].

Previous studies in SAW have shown that an excessive quantity of oxygen is initially added to the molten weld wire droplets from the arc cavity gas phase, up to 2000–3000 ppm O [4,5]. The word "excessive" as used in the prior statement means that the ppm O in the weld pool exceeds the solubility limit of oxygen in liquid steel at the cooling weld pool temperature. This is of importance, because once the welding head has moved forward there is no more arc energy input into the trailing weld pool, and it subsequently cools to lower temperatures from the high arc plasma temperatures that prevailed underneath the arc, typically 2000 to 2500 °C [7,8]. This initial excessive oxygen

quantity in the metal droplets is sourced from the decomposition of less stable oxides at the high temperatures prevailing in the arc plasma [9]. Based on the arc plasma stability hierarchy of oxides, the MnO, SiO_2, MgO and Al_2O_3 contained in the flux may dissociate in the arc plasma to release oxygen in the arc cavity to adsorb onto the molten weld wire droplets, reactions A to C in Figure 11 [9].

Previous works on SAW have shown that the excessive quantity of oxygen transferred from the arc cavity reacts with the molten steel at the arc plasma-weld pool interface to form FeO, reaction E. This FeO is incorporated into the slag. The correlation of increased FeO in the molten flux with increased weld metal total ppm O is well established and the slag FeO serves as an indicator of the oxygen potential prevailing at the molten flux-weld pool interface [16,35]. In our work, we apply aluminium powder to the SAW process to lower the oxygen potential prevailing at the molten flux-weld pool interface [26–33]. Similar to reaction G for reduction of MnO from the molten flux, FeO may also be reduced by aluminium, see Equation (4) in the text. These aluminium based reduction reactions, the reactions as displayed in Equations (2)–(5) in the text, are exothermic and therefore release chemical energy in the form of heat into the weld pool. This extra added heat can be used to melt and dissolve metal powder into the weld pool.

The reduced oxygen potential at the molten flux-weld pool interface prevents oxidation of chromium powder to CrO and Cr_2O_3 and also prevents oxidation of Co to CoO to prevent chromium and cobalt loss to the slag. Since Cr has a high affinity for oxygen the formation of CrO may occur at the arc plasma-weld pool interface, reaction E2. It is expected that this CrO would be reduced by aluminium according to the reaction similar to reaction G in Figure 11, the same as Equation (5) in the text in Section 3.1 [28,30]. Therefore, due to the chemical action of aluminium, the cobalt and chromium powders are melted and dissolved into the weld pool, see reactions I and M. Since there is an excess of Al added, some of the Al also dissolves directly into the weld pool, see reaction H.

Based on the results and discussion presented above it appears that chromium and cobalt loss in SAW, with the addition of metal powder alloying, occurs due to chromium and cobalt vaporisation and/or subsequent reaction of chromium and cobalt vapour with Fluorine gas to form $CrF_3(g)$ and $CoF_2(g)$. This reaction sequence is marked in Figure 11 as reactions J1 and K1 for cobalt reactions and as reactions J2 and K2 for chromium reactions, in combination with reaction L for $F_2(g)$ release from $CaF_2(g)$ dissociation. The formation of $F_2(g)$ in the arc cavity from the dissociation of $CaF_2(g)$ in the arc plasma appears possible, since the Ca and F were analysed in the arc cavity gas phase when a CaF_2 based flux was used in SAW test runs [1,42].

Aluminium vapour may react with the chromium and cobalt fluorides, $CrF_3(g)$ and $CoF_2(g)$, to transform these fluorides to cobalt and chromium vapour via reactions in Equations (11) and (12), presented by reactions M1 and M2 in Figure 11. Chromium and cobalt can be vaporised from the weld pool, at the arc plasma-weld pool interface, and from the unconstrained metal powders before dissolution of the metal powders into the weld pool. This conclusion is confirmed from the gas speciation calculation results from the FactSage 7.3 thermochemical software (Equilib module) gas-slag-metal powder calculations as summarised in Table 9.

The added aluminium powder plays a role in gas phase reactions in shifting chromium and cobalt powders to the vapour phase instead of oxidation of chromium and cobalt powders to CrO, Cr_2O_3 and CoO. However, the final arbiter of the oxidation state of chromium and cobalt is the partial oxygen pressure at the molten flux-weld pool interface because the final weld pool influencing reactions occur at this interface as the weld pool cools down from the high arc plasma temperatures to the weld pool solidus temperature.

The results presented here are in agreement with our previous similar works on the SAW process in which different metal powder combinations with aluminium were applied [26–33]. The results show that the oxygen potential at the molten flux-weld pool interface and in the arc cavity were lowered by aluminium powder addition. The importance of this effect of aluminium plays a critical role in the element transfer of

chromium and cobalt into the weld pool, without interfering with oxygen transfer from the plasma arc to the weld pool. The latter point in important in SAW because the target level of total ppm O is required in the weld metal to ensure acceptable materials properties in the weld metal. Previous chromium element transfer studies showed that the weld metal total ppm O can vary widely [16,17]. Cr_2O_3 containing flux formed weld metal with 470 ppm O to 1450 ppm O, and application of flux compositions of different BI values and containing zero Cr_2O_3 formed weld metal woth 230 ppm O to 700 ppm O [16,17]. This is in contrast to the typically low total oxygen content of 30 ppm O achieved in aluminium killed Cr-alloyed steel [43].

In summary, unconstrained aluminium metal powder was effectively applied with Co and Cr metal powders to control the weld metal total oxygen content by changing the original flux oxygen behaviour.

5. Conclusions

1. The flux oxygen behaviour is modified by the added aluminium powder through the lowering of the original flux induced partial oxygen pressure in the arc cavity and at the molten flux-weld pool interface.
2. Unconstrained metal powders of Al, Cr and Co were successfully applied in SAW to alloy carbon steel weld metal.
3. Higher Co yield from the metal powder to the weld metal was achieved in the presence of Cr at 81% Co vs. 70% Co in the absence of Cr.
4. Vapour formation and re-condensation of Si-Na-K-Fe-Mn-Co-Cr oxy-fluoride spheres (sized less than 10 μm) and smaller Si-Al-Ca-Mg-Na-K-Fe-Mn-Co-Cr oxy-fluoride needles occurred, as displayed in 3D slag sample EDX analyses.
5. Application of unconstrained metal powders in SAW can improve overall process productivity by removing the need for manufacturing of alloyed wire and alloyed powder as expensive time-consuming steps.

Author Contributions: F.D.B. as inventor conceptualised the work; F.D.B. and T.C. executed the experiments together, and interpreted the data together, and prepared the manuscript together. All authors have read and agreed to the published version of the manuscript.

References

1. Sengupta, V.; Havrylov, D.; Mendex, P.F. Physical phenomena in the weld zone of submerged arc welding—A Review. *Weld. J.* **2019**, *98*, 283–313.
2. O'Brien, A. *Welding Handbook—Materials and Applications, Part 1*, 9th ed.; American Welding Society (AWS): Miami, FL, USA, 2011; Volume 4.
3. Dallam, C.B.; Liu, S.; Olson, D.L. Flux composition dependence of microstructure and toughness of submerged arc HSLA weldments. *Weld. J.* **1985**, *64*, 140–152.
4. Polar, A.; Indacochea, J.E.; Blander, M. Electrochemically generated oxygen contamination in submerged arc welding. *Weld. J.* **1990**, *69*, 68–74.
5. Lau, T.; Weatherly, G.C.; Mc Lean, A. The sources of oxygen and nitrogen contamination in submerged arc welding using CaO-Al_2O_3 based fluxes. *Weld. J.* **1985**, *64*, 343–347.
6. Eagar, T.W. Sources of weld metal oxygen contamination during submerged arc welding. *Weld. J.* **1978**, *57*, 76–80.
7. Chai, C.S.; Eagar, T.W. Slag-metal equilibrium during submerged arc welding. *Metall. Trans. B* **1981**, *12*, 539–547. [CrossRef]
8. Mitra, U.; Eagar, T.W. Slag-metal reactions during welding: Part I. Evaluation and reassessment of existing theories. *Metall. Trans. B* **1991**, *22*, 65–71. [CrossRef]
9. Chai, C.S.; Eagar, T.W. Slag metal reactions in binary CaF_2-metal oxide welding fluxes. *Weld. J.* **1982**, *61*, 229–232.

10. Tuliani, S.S.; Boniszewski, T.; Eaton, N.F. Notch toughness of commercial submerged arc weld metal. *Weld. Met. Fabr.* **1969**, *37*, 327–339.

11. Palm, J.H. How fluxes determine the metallurgical properties of Submerged Arc Welds. *Weld. J.* **1972**, *51*, 358–360.

12. Paniagua-Mercado, A.M.; Lopez-Hirata, V.M.; Saucedo Munoz, M.L. Influence of the chemical composition of flux on the microstructure and tensile properties of submerged-arc welds. *J. Mater. Proc. Technol.* **2005**, *169*, 346–351. [CrossRef]

13. Bang, K.; Park, C.; Jung, H.; Lee, J. Effects of flux composition on the element transfer and mechanical properties of weld metal in submerged arc welding. *J. Met. Mater. Int.* **2009**, *15*, 471–477. [CrossRef]

14. Singh, B.; Khan, Z.A.; Siddiquee, A.N. Effect of flux composition on element transfer during Submerged Arc Welding (SAW): A literature review. *Int. J. Curr. Res.* **2013**, *5*, 4181–4186.

15. O'Brien, A. *Welding Handbook—Welding Processes, Part 1*, 9th ed.; American Welding Society (AWS): Miami, FL, USA, 1994; Volume 2.

16. Mitra, U.; Eagar, T.W. Slag metal reactions during submerged arc welding of alloy steels. *Metall. Trans. B* **1984**, *15*, 217–227. [CrossRef]

17. Burck, P.A.; Indacochea, J.E.; Olson, D.L. Effects of welding flux additions on 4340 steel weld metal composition. *Weld. J.* **1990**, *69*, 115–122.

18. Hybrid Welding: More Emissions Than with WIG and MIG Welding. Available online: https://safe-welding.com/laser-welding-automated-but-hazardous-for-employees-nonetheless/ (accessed on 8 July 2022).

19. Helis, L.; Toda, Y.; Hara, T.; Miyazaki, H.; Abe, F. Effect of cobalt on the microstructure of tempered martensitic 9Cr steel for ultra-supercritical power plants. *Mater. Sci. Eng. A* **2009**, *510–511*, 88–94. [CrossRef]

20. Jing, H.; Luo, Z.; Xu, L.; Zhao, L.; Han, Y. Low cycle fatigue behavior and microstructure of a novel 9Cr-3W-3Co tempered martensitic steel at 650 °C. *Mater. Sci. Eng. A* **2018**, *731*, 394–402. [CrossRef]

21. Hallén, H.; Johansson, K.-E. Use of a Metal Powder for Surface Coating by Submerged Arc Welding. U.S. Patent 6331688 B1, 18 December 2001.

22. Daily Metal Price. Available online: https://www.dailymetalprice.com/ (accessed on 11 July 2022).

23. Hercik, T.; Sigmund, M.; Hruby, P. Weldability of cobalt alloys by hybrid methods. *MM Sci. J.* **2021**, *2021*, 4946–4953. [CrossRef]

24. Raabe, D.; Tasan, C.C.; Springer, H.; Bausch, M. From high-entropy alloys to high-entropy steels. *Steel Res. Int.* **2015**, *86*, 1127–1138. [CrossRef]

25. Moon, J.; Ha, H.-Y.; Kim, K.-W.; Park, S.-J.; Lee, T.-H.; Kim, S.-D.; Jang, J.H.; Jo, H.-H.; Hong, H.-U.; Lee, B.H.; et al. A new class of lightweight, stainless steels with ultra-high strength and large ductility. *Sci. Rep.* **2020**, *10*, 12140. [CrossRef]

26. Coetsee, T.; De Bruin, F. Aluminium Assisted Nickel Alloying in Submerged Arc Welding of Carbon Steel: Application of Unconstrained Metal Powders. *Appl. Sci.* **2022**, *12*, 5392. [CrossRef]

27. Coetsee, T.; De Bruin, F.J. Improved titanium transfer in Submerged Arc Welding of carbon steel through aluminium addition. *Miner. Process. Extr. Metall. Rev.* **2021**, *43*, 771–774. [CrossRef]

28. Coetsee, T.; De Bruin, F.J. Reactions at the molten flux-weld pool interface in submerged arc welding. *High Temp. Mater. Processes.* **2021**, *40*, 421–427. [CrossRef]

29. Coetsee, T.; De Bruin, F. Application of Copper as Stabiliser in Aluminium Assisted Transfer of Titanium in Submerged Arc Welding of Carbon Steel. *Processes* **2021**, *9*, 1763. [CrossRef]

30. Coetsee, T.; De Bruin, F. Chemical Interaction of Cr-Al-Cu Metal Powders in Aluminum-Assisted Transfer of Chromium in Submerged Arc Welding of Carbon Steel. *Processes* **2022**, *10*, 296. [CrossRef]

31. Coetsee, T.; De Bruin, F. Aluminium-Assisted Alloying of Carbon Steel in Submerged Arc Welding: Application of Al-Cr-Ti-Cu Unconstrained Metal Powders. *Processes* **2022**, *10*, 452. [CrossRef]

32. Coetsee, T.; De Bruin, F. Application of Unconstrained Cobalt and Aluminium Metal Powders in the Alloying of Carbon Steel in Submerged Arc Welding: Thermodynamic Analysis of Gas Reactions. *Appl. Sci.* **2022**, *12*, 8472. [CrossRef]

33. Coetsee, T.; De Bruin, F. Aluminium-Assisted Alloying of Carbon Steel in Submerged Arc Welding with Al-Cr-Ni Unconstrained Metal Powders: Thermodynamic Interpretation of Gas Reactions. *Processes* **2022**, *10*, 2265. [CrossRef]

34. Coetsee, T. Phase chemistry of Submerged Arc Welding (SAW) fluoride based slags. *Mater. Res. Technol.* **2020**, *9*, 9766–9776. [CrossRef]

35. Coetsee, T.; Mostert, R.J.; Pistorius, P.G.H.; Pistorius, P.C. The effect of flux chemistry on element transfer in Submerged Arc Welding: Application of thermochemical modelling. *Mater. Res. Technol.* **2021**, *11*, 2021–2036. [CrossRef]

36. Bale, C.W.; Bélisle, E.; Chartrand, P.; Decterov, S.; Eriksson, G.; Gheribi, A.E.; Hack, K.; Jung, I.-H.; Kang, Y.-B.; Melançon, J.; et al. Reprint of: FactSage thermochemical software and databases, 2010–2016. *Calphad* **2016**, *55*, 1–19. [CrossRef]

37. Coetsee, T.; De Bruin, F. In Situ Modification of CaF_2-SiO_2-Al_2O_3-MgO Flux Applied in the Aluminium-Assisted Transfer of Titanium in the Submerged Arc Welding of Carbon Steel: Process Mineralogy and Thermochemical Analysis. *Minerals* **2022**, *12*, 604. [CrossRef]

38. Coetsee, T.; De Bruin, F. Insight into the Chemical Behaviour of Chromium in CaF_2-SiO_2-Al_2O_3-MgO Flux Applied in Aluminium-Assisted Alloying of Carbon Steel in Submerged Arc Welding. *Minerals* **2022**, *12*, 1397. [CrossRef]

39. Kluken, A.O.; Grong, Ø. Mechanisms of inclusion formation in Al-Ti-Si-Mn deoxidized steel weld metals. *Metall. Trans. B* **1989**, *20*, 1335–1349. [CrossRef]

40. Lau, T.; Weatherly, G.C.; Mc Lean, A. Gas/Metal/Slag reactions in Submerged Arc Welding using CaO-Al$_2$O$_3$ based fluxes. *Weld. J.* **1986**, *65*, 31–38.

41. Mitra, U.; Eagar, T.W. Slag-metal reactions during welding: Part II. Theory. *Metall. Trans. B* **1991**, *22*, 73–81. [CrossRef]

42. Gött, G.; Gericke, A.; Henkel, K.-M.; Uhrlandt, D. Optical and spectroscopic study of a submerged arc welding cavern. *Weld. J.* **2016**, *95*, 491–499.

43. Lee, S.-B.; Choi, J.-H.; Jung, S.-M.; Lee, H.-G.; Rhee, P.C.H. Aluminium deoxidation equilibrium on liquid Fe-16 Pct Cr alloy. *Metall. Trans. B* **2005**, *36*, 414–416. [CrossRef]